DESIGN AND SIMULATION ANALYSIS OF A SIX-WHEELED RESCUE ROBOT

Hengzheng LI[1], Lei YANG[2*], Yue HAN[3], Jie YANG[4], Conghu LIU[5], Yin ZHANG[6*]

The complex on-site environment after a disaster is often the main factor hindering rescue workers from carrying out timely rescue work. This article designs a six- wheel rescue robot with a rocker arm bogie structure. The robot uses the rear wheels as the steering gear, and each wheel is independently driven, which has good flexibility and obstacle crossing ability. The simulation test of ADAMS shows that after optimizing the robot body size, it can pass over a vertical obstacle model with a height of 250 mm, meeting the preset passing requirement of 200 mm. Compared with robots without control optimization, robots using drive-time function control have smoother and more accurate steering, and their steering performance has been improved significantly.

Keywords: rescue robot, rocker arm-bogie structure, dynamic simulation

1. Introduction

The complex on-site environment and risk uncertainty after a disaster have brought enormous difficulties to post disaster rescue. Using remote controlled robots to investigate and search can better help rescue workers quickly clear the situation at the scene after the disaster, reducing the work intensity and rescue risks of rescue workers [1-3]. In order to develop rescue robots suitable for various types of disaster scenes, scholars have conducted a lot of research on rescue robots, and have achieved certain results. The existing land rescue robots can be divided into three types in terms of configuration: foot type, wheel type, and crawler type [4]. The footed robot has strong obstacle surmounting ability and flexibility in post

[1] Ass. Prof., School of Mechanical and Electronic Engineering, Suzhou University, Suzhou 234000, China, e-mail: lihengzheng0216@foxmail.com
[2] Stu., School of Mechanical and Electronic Engineering, Suzhou University, Suzhou 234000, China, Correspondence e-mail: 2690585359@qq.com
[3] Stu., School of Mechanical and Electronic Engineering, Suzhou University, Suzhou 234000, China, e-mail: 3084336346@qq.com
[4] Ass. Prof., School of Mechanical and Electronic Engineering, Suzhou University, Suzhou 234000, China, e-mail: 304902927@qq.com
[5] Prof., School of Mechanical and Electronic Engineering, Suzhou University, Suzhou 234000, China, e-mail: liuconghu@sjtu.edu.cn
[6] Lectr., School of Mechanical Engineering, Anhui University of Science and Technology, Huainan, 232001, China, Correspondence e-mail: zhangyin@aust.edu.cn

disaster scenarios, but its movement speed is low, the high center of gravity leads to easy rollover and insufficient stability [5,6]. Wheeled robots have strong mobility but rely more on structured road, which has limitations in dealing with complex on-site environments after disasters [7,8]. Crawler type robots have good obstacle surmounting ability and high flexibility, but poor movement ability [9-10]. As shown in Fig. 1 (a), the "Ruins search and assistance rescue robot" designed and developed by the Shenyang Institute of Automation, Chinese Academy of Sciences is equipped with a color camera and thermal imager, which can better adapt to search work under collapsed buildings. Fig. 1 (b) is a "Kinect" earthquake rescue robot designed and developed by the University of Warwick in the United Kingdom, which is equipped with a range finder capable of transmitting three-dimensional image data in real time. Fig. 1 (c) shows the "Quince" rescue robot at Chiba University of Technology in Japan. The robot is equipped with infrared sensors and carbon dioxide sensors, which can detect the respiration and temperature of personnel on the scene after the disaster, providing assistance for rescue personnel in their search.

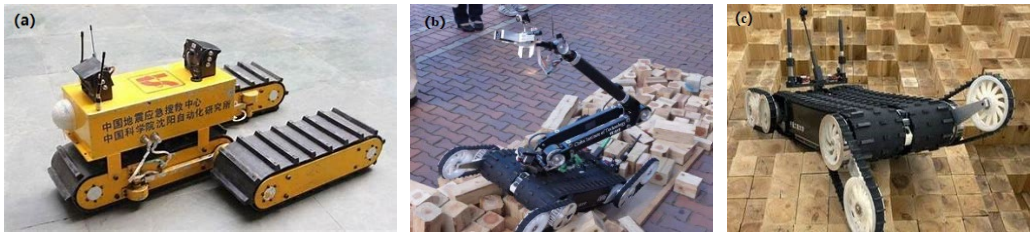

Fig. 1. Typical rescue robot: (a) "Ruin search and assisted rescue robot", (b) "Kinect" earthquake rescue robot, (c) "Quince" rescue robot.

Although the above rescue robots have provided significant assistance in disaster rescue, there are still significant application limitations for rescue robots. On the one hand, the collapse of obstacles in the post disaster scene limits the use of some rescue robots. On the other hand, rescue robots still need significant improvements in their travel speed and turning performance. At present, the performance requirements for mobile rescue robots are mainly reflected in aspects such as smoothness of travel, obstacle surmounting, normal travel speed, endurance, and adaptive ground capabilities [11-15]. Aiming at the problems existing in the current application of land rescue robots, this paper designs a six-wheeled rescue robot with a rocker bogie, and completes the structural design and motion simulation analysis of the robot. The relevant research in this article can provide a theoretical reference for the design and development of high-speed and high-trafficability rescue robots.

2. Overall Design of the Six-wheeled Rescue Robot

2.1 Overall Structural Design

The six-wheeled rescue robot is composed of robot body, center differential, main rocker arm, auxiliary rocker arm, drive motor, rear wheel steering gear and wheels. Its overall structure is shown in Figure 2.

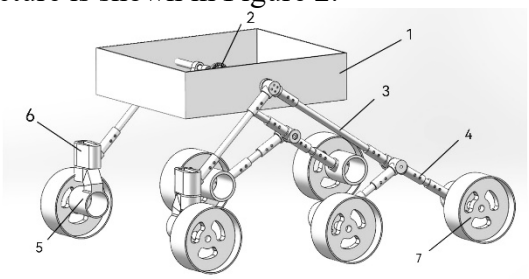

1. Robot body, 2. Center differential, 3. Main rocker arm, 4. Auxiliary rocker arm, 5. Drive motor, 6. Rear wheel steering gear, 7. Wheels

Fig. 2. Overall schematic diagram of the robot

The overall structure of the robot is a rocker arm-bogie. A triaxial center differential is installed on the robot body. The side shaft of the differential is locked with the main rocker arm of the robot body, and the longitudinal shaft fits with the bearing seat on the robot body. The center differential can ensure the balance of the robot body when the rocker arms on both sides rotate. The main rocker arms are symmetrically distributed on both sides of the robot body. The rear end of the main rocker arm is connected to the rear wheel steering gear, and the front end is connected to the auxiliary rocker arm. The cooperation of the main and auxiliary rocker arms ensures the obstacle passing ability of the robot. The rear wheel steering actuator is the steering mechanism of a robot, which controls the active deflection of the rear wheel through a servo mechanism to achieve the purpose of steering. The robot traveling method adopts a centralized control distributed drive method. A drive mechanism is installed at the ends of the steering mechanism and the auxiliary rocker arm. A central control element installed on the vehicle body controls the rotation speed of the drive motor. This driving method has a simple structure and is conducive to giving full play to the kinematic performance and portability of the robot [16-21]. In order to ensure the flexibility and obstacle passing ability of the robot, and to integrate the actual working environment of the robot, the overall structural dimensions of the six-wheeled rescue robot are shown in Fig. 3.

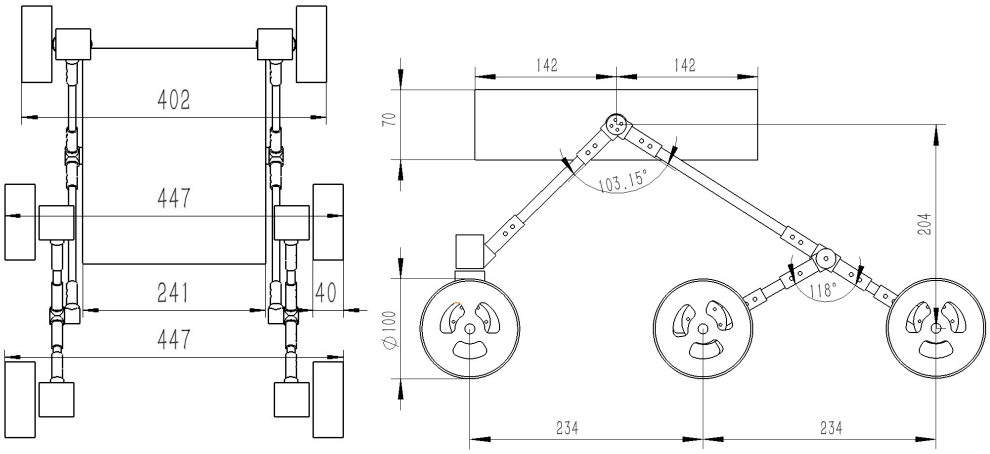

Fig. 3. Overall dimension parameters of the robot

2.2 Design of Robot Steering Control

When the six-wheeled rescue robot moves forward and backward in a straight line, its left and right wheels rotate at the same speed. When turning is required during driving, due to the absence of a steering differential in the robot body structure and the independent drive of each wheel, the vehicle body is prone to slip or drag during cornering. In order to ensure the turning performance of the robot, it is necessary to control the rotational speed of each wheel. When the robot turns, the radians swept by the wheel trains on both sides of the robot are the same, that is, the angular speed ω and movement time t of both sides are the same, and the relationship formula between the angular velocity and the linear velocity is satisfied:

$$v = \omega r \tag{1}$$

Where v is the wheel rotational speed, unit: m/s. ω is the angular speed of the robot body turning, units: rad/s. r is the distance from the wheel to the steering center, unit: m.

From Equation (1), the proportional relationship between the rotational speed v of each wheel and the distance r from each wheel to the steering center can be obtained. From the relationship between steering angle and steering radius [22]:

$$r = \frac{L}{\sin\theta} \tag{2}$$

Where L is the overall length of the robot, unit: m. θ is the steering angle, unit: rad.

The geometric relationship of each wheel of the robot is shown in Figure 4. Taking point o as the steering center, the linear speed of wheel 2 is expressed as v_2 and its speed is defined as 1. By combining Formula (1) and Formula (2), the output speed relationship of each wheel during steering can be obtained:

$$v_{\mathrm{n}} = v_2 \frac{R_{\mathrm{n}}}{R_2} \tag{3}$$

Where n is the wheel number.

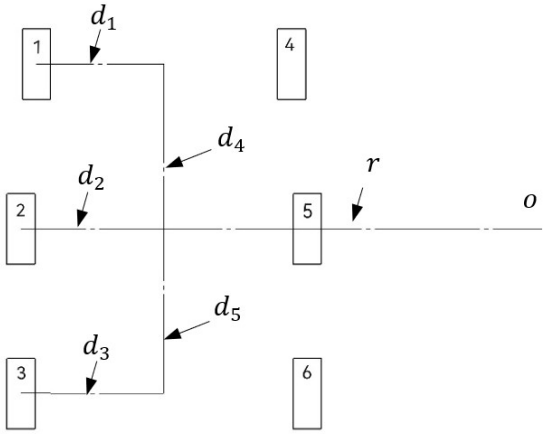

Fig. 4. Schematic diagram of geometric relationship of each wheel

In Fig. 4, d_1, d_2, d_3 is the half axle length of the front, middle, and rear axles, d_4, d_5 is the length between the front and rear axles and the middle axle. Substituting the geometric dimension relationship in Fig. 4 into Equation 3 can obtain the speed relationship formula for each wheel:

$$v_1 = v_2 \frac{r_1}{r_2} = \frac{\sqrt{d_4^2+(d_1+r)^2}}{r+d_2} \tag{4}$$

$$v_2 = 1 \tag{5}$$

$$v_3 = v_2 \frac{r_3}{r_2} = \frac{\sqrt{d_5^2+(d_3+r)^2}}{r+d_2} \tag{6}$$

$$v_4 = v_2 \frac{r_4}{r_2} = \frac{\sqrt{d_4^2+(r-d_1)^2}}{r+d_2} \tag{7}$$

$$v_5 = v_2 \frac{r_5}{r_2} = \frac{r-d_2}{r+d_2} \tag{8}$$

$$v_6 = v_2 \frac{r_6}{r_2} = \frac{\sqrt{d_5^2+(r-d_3)^2}}{r+d_2} \tag{9}$$

Substituting the actual size data of the robot into Equation (4) - (9) can obtain the proportional function of the output speed of each wheel when the robot turns, as shown in Table 1. Compiling the obtained function into its control code can achieve control of the output speed of each wheel of the robot.

Table 1

Speed proportional function of each wheel of the robot

Wheel number	Velocity proportional function
1	$\frac{\sqrt{506.25-45\sqrt{r_3^2-234^2}+r_3^2}}{\sqrt{r_3^2-234^2}}$
2	1
3	$\frac{r_3}{\sqrt{r_3^2-234^2}}$
4	$\frac{\sqrt{147840.25-769\sqrt{r_3^2-234^2}+r_3^2}}{\sqrt{r_3^2-234^2}}$
5	$\frac{-407+\sqrt{r_3^2-234^2}}{\sqrt{r_3^2-234^2}}$
6	$\frac{\sqrt{165649-814\sqrt{r_3^2-234^2}+r_3^2}}{\sqrt{r_3^2-234^2}}$

3. Simulation and Optimization of Six-wheeled Robot

3.1 Simulation of robot obstacle crossing

According to the design size requirements of the rescue robot, the SolidWorks software is used for modeling. After modeling, import the model into the database of Adams software, create a gravity coordinate system, and determine the centroid and reference marker points of each component. Define the material type of each component to ensure quality consistency. Create three vertical obstacle models (height: 150 *mm*, 200 *mm*, 250 *mm*) and add it to the ground environment. Add corresponding motion pair connections to the components to ensure that the model can move according to the design and ensure corresponding motion relationships during simulation. The simulation parameter settings for the robot during the motion simulation process are shown in Table 2.

Table 2

Robot Motion Simulation Parameters [23-27]

Parameter	Numerical value
Rigidity	1.0E+05 *N/m*
Force index	2.2
damping	10.0 *N·s/m*
Penetration depth	0.1 *mm*
Static friction coefficient	0.71
Dynamic friction coefficient	0.4

Since the robot is driven independently by six wheels, it is necessary to apply the same rotational pair drive to each of the six-wheeled rotational pairs, and define its driving time function (*150 d*time*). Where, *d* is the rotation angle of the wheel rotation pair, and the unit is °; *time* is the rotational time of the wheel, and the unit is *s*. The meaning of (*150 d*time*) is that the wheel drive motor rotates 150° per second. After the preparation work is completed, perform motion simulation on the robot model, and set the simulation time to 15 *s*. The simulation results of the 150 *mm* vertical obstacle show that the first four wheels of the robot successfully surmounted the obstacle, but the subsequent two wheels skidded on the vertical plane, causing it to be unable to surmount the obstacle. The centroid of the left rear wheel of the robot is taken as the measurement object, and the geodetic coordinate system is used as the reference coordinate system to measure its moving length. The displacement and force curve of the six-wheeled robot is shown in Figure 5. In the figure, the X axis represents the forward displacement of the robot, and the Y axis represents the effective component force and movement displacement of the robot in the obstacle crossing direction. As can be seen from the figure, when the rear wheels start to climb over vertical obstacles, the contact force begins to appear, but the peaks on the force curve are relatively discrete and the value is low. The Y-axis displacement component curve is shown as a wave curve, and the robot reciprocates up and down on the vertical plane of the obstacle. It is speculated that the reason may be that the center of gravity of the robot's body platform is located on the central axis of the main cantilever, causing the center of gravity of the entire robot to deviate. It is speculated that the reason may be that the center of gravity of the robot is located on the central axis of the main cantilever, causing the center of gravity of the entire robot to deviate from the rear. When the robot climbs over the vertical obstacle, the rear center of the robot causes a small contact force between the wheel and the obstacle surface, which is insufficient to provide the driving force for the robot to continue its upward movement.

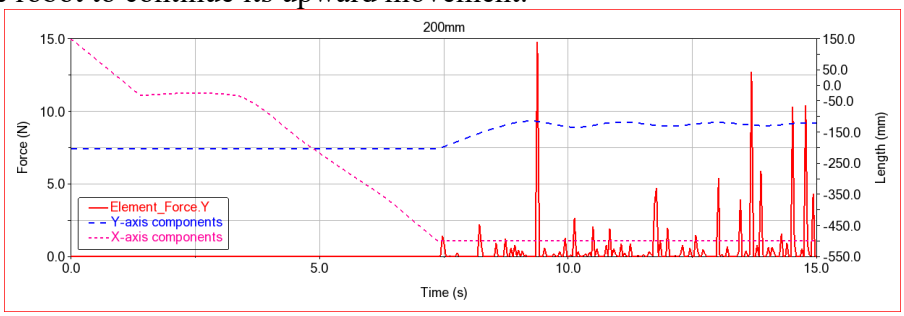

Fig. 5. Displacement and force curve of robot passing over obstacles before optimization

3.2 Optimal design of robot structure

Without changing the motion relationships and overall dimensions of the existing components of the robot, it is an inevitable choice to optimize the robot structure so that the robot can pass over vertical obstacles with a height of 200 *mm*. From the previous simulation analysis, it can be seen that the robot's inability to pass the obstacle with a height of 150 *mm* may be caused by its center of gravity being behind. Taking the central axis of the robot's main cantilever as the center, the body platform is optimized from symmetrical distribution to a front length of 224 *mm* and a rear length of 112 *mm*. The optimized forward movement of the robot's center of gravity can reduce the lift required by the rear wheels when the robot climbs vertical obstacles, achieving the goal of improving its passing ability. Similarly, three height obstacles (150 *mm*, 200 *mm*, and 250 *mm*) were set up, with a simulation time of 15 *s*. The optimized model was simulated multiple times, and all obstacles successfully passed over.

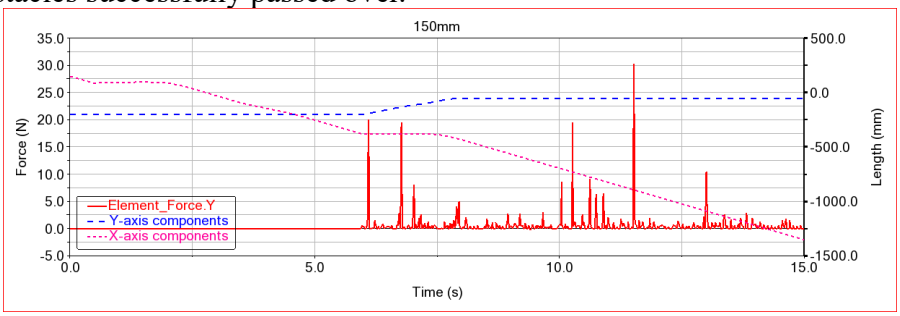

Fig. 6. Displacement and force curve of the model over 150 *mm*

Fig. 6 shows the displacement and force curve of the model over 150 *mm* obstacle. From the figure, it can be seen that during the process of climbing, the displacement of the robot in the X-axis and Y-axis directions changes smoothly without obvious fluctuations. The climbing force in the Y-axis direction of the wheels has significantly improved. The process of robot climbing over obstacles is shown in Figure 7. Fig. 7 (a) shows that the four front wheels of the robot model are about to climb over the obstacle, while the rear wheels are still advancing on the ground. Fig. 7 (b) shows that the four front wheels of the robot model have climbed over the obstacle, and the rear wheels are in the process of climbing over the obstacle; Fig. 7 (c) shows that all six wheels of the robot model have crossed the obstacle and advanced on it, indicating that the robot model has successfully passed the vertical obstacle set.

Fig. 7. Obstacle crossing process of the six-wheeled robot: (a) the front wheels are about to climb over the obstacle (b) the front wheels have crossed the obstacle (c) completed climbing the obstacle

In order to explore the passing performance of the optimized model, this paper also simulated the process of the robot passing over the 250 *mm* obstacle. The displacement and force curve of the model over 250 *mm* is shown in Figure 8. From the image, it can be clearly seen that after the optimized robot rear wheel contacts the vertical surface of the obstacle, the contact force generated is denser than the contact force of the original model, and the force value is larger, providing sufficient lifting force for the robot to pass over the obstacle.

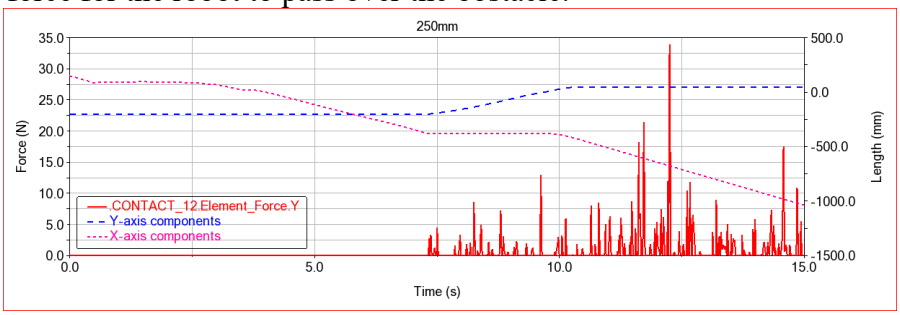

Fig. 8. Displacement and force curve of the model over 250 *mm*

Simulation results have shown that the assumption that the robot cannot successfully cross vertical obstacles before optimization is correct. By changing the center of gravity of the robot, the six-wheeled robot can surmount the vertical obstacle with a height of 250 *mm*, which better meets the preset performance requirements.

3.3 Simulation of six-wheeled robot steering control

Conduct steering simulation on the optimized structural model, and set the maximum deflection angle of both rear wheels to 30° [13, 27]. Define the drive time function of the wheel 2 rotation pair as (*100 d*time*). According to the scale function in Table 1, obtain the drive time function for each wheel as shown in Table 3.

Table 3

Steering drive time function

Wheel number	Numerical value
1	*100.21 d*time*
2	*100.00 d*time*
3	*102.19 d*time*
4	*66.92 d*time*
5	*63.39 d*time*
6	*66.79 d*time*

In order to clarify the effect of the drive time function on the improvement of the robot's steering performance, the steering simulation uses a model without the drive time function as a control group (that is, drive time function of the six wheels is all (*100 d*time*)). The optimization method for steering motion simulation uses the steering drive time function in Table 3. Using the centroid of wheel 3 as the measurement point, the geodetic coordinate system as the reference coordinate system, and the XOZ plane as the motion plane, measure the motion curve of wheel 3 on the Z axis. The turning motion curve of the six-wheeled robot before and after optimization using the drive time function is shown in Fig. 9.

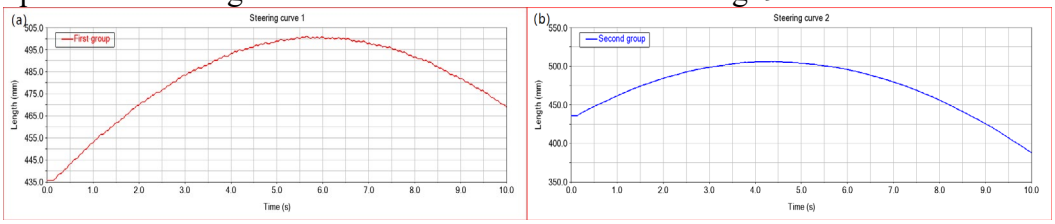

Fig. 9. Turning motion curve: (a) before optimization, (b) after optimization

Comparing Figure 9 (a) and 9 (b), it is evident that the simulation image optimized by the drive time function is smoother and closer to the standard arc compared to the unoptimized simulation image. This shows that the steering controllability using the drive function designed is significantly higher than that without steering optimization.

4. Conclusions

This article designs a six-wheel rescue robot with a rocker bogie structure and uses Adams software to simulate and analyze the model. The obstacle crossing motion simulation shows that the backward shift of the vehicle center of gravity is the main reason why the vehicle cannot pass over a vertical obstacle with a height of 150 *mm*. After optimizing the body size of the robot, its passing ability is significantly improved, and it can pass over a vertical obstacle model with a height of 250 *mm*, meeting the preset passing requirement of 200 *mm*. The simulation of turning motion shows that when the robot using drive time function control performs steering, its steering is smoother and more accurate, and its steering performance is better improved compared to the robot without control optimization.

Although the relevant research in this article provides a certain reference for the design and development of the six-wheeled robot with a rocker arm, it only simulates and analyzes the robot's passing ability when facing block shaped obstacles. There are still shortcomings in research on the passing ability of asymmetric obstacles (such as stones) and the stability of the vehicle body during passing. In future research, we will continue to conduct relevant research with the requirement of passing over asymmetric obstacles.

Acknowledgments

This work was supported by the Scientific Research Foundation for Doctoral of Suzhou University (2020BS009, 2013YKF24), the Natural Science Research Project in Universities of Anhui Province in China (2022AH051386), Anhui Higher Education Quality Engineering Project (2022jyxm1595, 2020gnxm070, 2021jyxm1502, 2020mooc566), Student Innovation and Entrepreneurship Training Project of Anhui (KYLXYYBXM22-188).

REFERENCES

[1]. *R. K. Megalingam, S. R. Vadivel, A. A. Rajendraprasad, S. Baskar and M. R. Balasubramani,* "Development and evaluation of a search-and-rescue robot Paripreksya 2.0 for WRS 2020", in Adv. Rob., **vol. 36**, no. 21, Sept. 2022, pp. 1120-1133.

[2]. *S. J. Armando, A. J. Aníbal, T. Hiroshi and P. A. Elías,* "Staircase Detection, Characterization and Approach Pipeline for Search and Rescue Robots", in Appl. Sci., **vol. 11**, no. 22, Nov. 2021, 10736-10736.

[3]. *M. D. Moniruzzaman, R. Z. Saniat, R. Sabbir, M. Sanwar and S. Antar,* "Design and Implementation of Urban Search and Rescue Robot", in Int. J. Eng. Manuf., **Vol. 8**, no. 2, Mar. 2018, pp. 12-20.

[4]. *L. Bai, J. Guan, X. H. Chen, J. Z. Hou, W. B. Duan,* "An optional passive/active transformable wheel-legged mobility concept for search and rescue robots", in Rob. Auton. Syst., **Vol. 107**, Sept. 2018, pp. 145-155.

[5]. *A. Shadi and K. Kathryn,* "Motion behavior recognition dataset collected from human perception of collective motion behavior", in Data Brief, **vol. 47**, no. 47, Feb. 2023, pp.108976-108976.

[6]. *T. H. Kim, S. H. Bae, C. H. Han, B. Hahn* "The Design of a Low-Cost Sensing and Control Architecture for a Search and Rescue Assistant Robot", in Machines, **vol. 11**, no. 3, Feb. 2023, pp.329-329.

[7]. *Y. T. Li, C. J. Wang and C. J. Zhang,* "Optimization of the suspension system and analysis of the ride performance of the crawler-type coal mine search and rescue robot", in J. Braz. Soc. Mech. Sci. Eng., **vol. 44**, no. 5, Apr. 2022, pp. 167-181.

[8]. *J. B. Qian, Z. R. Xu, Y. Y. Luo, N. Pan, Y. Liu and W. H. Hsieh,* "Design and implementation of underwater search for salvage robot power system", in J. Intell. Fuzzy Syst., **vol. 40**, no. 4, Apr. 2021, pp. 7819-7828.

[9]. *T. Kamegawa, T. Akiyama, S. Sakai, K. Fujii, K. Une, E. Ou, Y. Matsumura, T. Kishutani, E. Nose, Y. Yoshizaki and A. Gofuku,* "Development of a separable search-and-rescue robot

composed of a mobile robot and a snake robot", in Adv. Rob., **vol. 34**, no. 2, Nov. 2020, pp.132-139.
[10]. *B. Robert,* "Disaster relief, and search and rescue robots: the way forward", in Ind. Rob., **vol. 46**, no. 2, Apr. 2019, pp.181-187.
[11]. *L. A. Cartal, V. I. Gheorghe, A. Rotaru, D. Duminica, S. Petrache,* "Developing a new mobile robotic structure for search and rescue operations", in IOP Conf. Ser.: Mater. Sci. Eng., **vol. 444**, no. 4, Sept. 2018, pp. 42016-42016.
[12]. *M. Evgeni, M. Fumitoshi, S. Jackrit, S. Mikhail, B. Yang, T. Tatyana, S. Ramil, L. Roman, Z. Aufar, N. Hiroaki, H. Michinori and E. Takahiro,* "e-ASIA Joint Research Program: development of an international collaborative informational system for emergency situations management of flood and land slide disaster areas", in Artif. Life Rob., **vol. 27**, no. 4, Oct. 2022, pp. 613-623.
[13]. *V. M. Rafael, C. S. Jose, A. H Abel, M. A. Andres, G. M. Joseph, G. B. Jarelh and T. S. Jesus,* "Development of a Low-Cost Teleoperated Explorer Robot (TXRob)", in Int. J. Adv. Comput. Sci. Appl., **vol. 13**, no. 7, Jul. 2022, pp. 897-903.
[14]. *C. A. Jeyson, L. C. Samuel, C. C. Juan and T. S. Jesus,* "Analysis of the Intuitive Teleoperated System of the TxRob Multimodal Robot", in Int. J. Adv. Comput. Sci. Appl., **vol. 13**, no. 10, Oct. 2022, pp. 782-788.
[15]. *O. Andersson, P. Doherty, M. Lager, J. O. Lindh, L. Persson, E. A. Topp, J. Tordenlid and B. Wahlberg,* "WARA-PS: a research arena for public safety demonstrations and autonomous collaborative rescue robotics experimentation", in Auton. Intell. Syst., **vol.1**, no. 1, Nov. 2021, pp.1-31.
[16]. *Shang, Zuen*, The Design and Properties Research of the Foldable Waterbomb Wheel Structure of the Coal Mine Rescue Robot. PhD Thesis, Liaoning Technical University, 2021.
[17]. *S. Hong, G. Park, Y. Lee and S. Kang*, "Design and Control Strategy for Rescue Robot to Execute Rescue Missions in a Highly Unstructured Environment", in J. Inst. Control Rob. Syst., **vol. 26**, no. 8, Aug. 2020, pp. 683-695.
[18]. *M. Hatano, T. Fujii,* "3-D shape recognitions of target objects for stacked rubble withdrawal works performed by rescue robots", in Artif. Life Rob., **vol. 25**, no, 1, Oct. 2020, pp. 94-99.
[19]. *X. J. Li, J. Liang and H. Q. Li*, "Design of earthquake rescue robot based on AHP /QFD and TRIZ", in J. Mach. Des., **vol. 38**, no. 11, Nov. 2021, 38, pp.121-128.
[20]. *X. Z. Zheng, J. Zhao and D. Zhang*, "Research Status and Development Trend of Coal Mine Rescue Robot", in Indu. Mine Autom., **vol. 45**, no. 9, Sept. 2019, pp.7-12.
[21]. *H. Xu and W. Z. Guo*, "Wheeled robots: innovation design and experiments", in J. Integr. Technol., **vol. 11**, no. 4, Apr. 2022, pp. 3-18
[22]. *P. Y. Shao, T. Wang and W. B. Dong*, "Research on structure design and parameter optimization of new wheeled mobile robot", in High Technol. Lett., **vol.32**, no.9, Sept. 2022, pp. 959-971.
[23]. *F. C. Wang, H. L. Gao and X. G. Song*, "Design and Manufacture of an All-Terrain Six Wheel Mobile Robot", in Mach. Des. Manuf., **vol. 5**, no. 5, May. 2020, pp. 253-256.
[24]. *M. Jayasudha and M. Saravanan*, "Real Time Implementation of Smart Child Rescue Robot from Bore Well using Arm and Belt Mechanism", in Int. J. Innovative Technol. Explor. Eng. **Vol. 8**, no, 12, Oct. 2019, pp.3346-3350.
[25]. *D. Jeffrey, M. Stefano, G. Alessandro, G. Boris, M. Kamilo, H. Tomislav, C. Cesar, H. Marco, I. Auke, D. Floreano, M. G. Luca, S. Roland and S. Davide*, "The current state and future outlook of rescue robotics", in J. Field Rob., **vol. 36**, no. 7, Aug. 2019, pp. 1171-1191.
[26]. *M. Yu, S. Y. Tong and L.* Y. Kong, "A Review of Tire-asphalt Pavement Friction Measurement and Skid Resistance Model Study", in J. Highw. Traffic Res. Dev., **vol. 37**, no. 10, Oct. 2020, pp. 12-24.
[27]. *Jinsheng Liu,* Modeling and simulation of six-wheel suspension rover based on ADAMS, PhD. Thesis, Beijing University of Posts and Telecommunications, 2019.